J. Fluid Mech. (2026), *vol.* 1029, A44, doi:10.1017/jfm.2026.11239

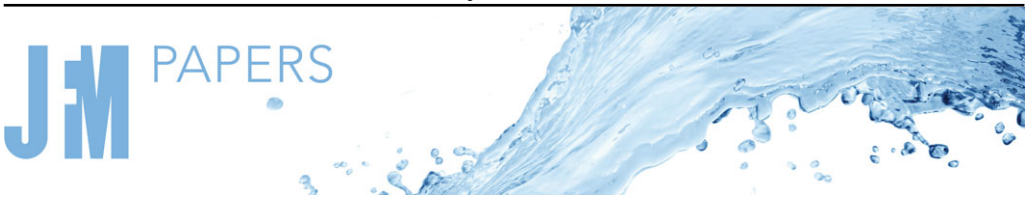

Local cusp solutions of viscous flow

Rodolfo Brandão[1,†], **Jens Eggers**[1] and **Marco Fontelos**[2]

[1]School of Mathematics, University of Bristol, Fry Building, Woodland Road, Bristol BS8 1UG, UK

[2]Instituto de Ciencias Matemáticas (ICMAT, CSIC-UAM-UCM-UC3M), C/ Serrano 123, 28006 Madrid, Spain

Corresponding author: Jens Eggers, jens.eggers@bristol.ac.uk

(Received 5 September 2025; revised 12 December 2025; accepted 22 January 2026)

Free-surface cusps are a generic feature of externally driven, viscous flow bounded by a free surface, in that their form is stable under small perturbations. Here we present an alternative to the boundary integral description found recently (J. Eggers, *Phys. Rev. Fluids*, vol. 8, 2023, 124001), which is based directly on a local analysis of the Stokes equation. The new description has the advantage of greater simplicity and transparency, allowing us to understand the connections with bifurcation theory, as well as with other physical systems displaying similar singularities. To illustrate this, we construct cusp solutions corresponding to higher-order singularities, as well as time-dependent solutions.

Key words: slender-body theory, capillary flows

1. Introduction

When a viscous fluid with a free surface is strongly driven, the free surface is often seen to deform into a cusp singularity, rounded at the tip on a small scale only. As long as the driving varies slowly in the third dimension, the tip position is close to a straight line, and the flow can be regarded as effectively two-dimensional. The formation of free-surface cusps was first highlighted and demonstrated experimentally by Joseph *et al.* (1991), placing two counter-rotating rollers beneath the free surface of a viscous fluid, dragging fluid into the space between them. The observed cusps were so sharp that it led Joseph *et al.* (1991) to propose that the free surface was indeed ending in a point, producing a non-differentiable surface even in the presence of surface tension.

[†]*Present address:* Department of Mathematics, University of British Columbia, Vancouver, BC V6T 1Z2, Canada.

© The Author(s), 2026. Published by Cambridge University Press. This is an Open Access article, distributed under the terms of the Creative Commons Attribution licence (https://creativecommons.org/licenses/by/4.0/), which permits unrestricted re-use, distribution and reproduction, provided the original article is properly cited.

https://doi.org/10.1017/jfm.2026.11239 Published online by Cambridge University Press

To investigate this question, Jeong & Moffatt (1992) constructed an exact solution to the two-dimensional viscous flow equations, driven by a vortex dipole underneath a free surface, using the method of complex mapping from the unit disk into the flow domain. They found that the tip size remains finite, but is exponentially small in the capillary number, which is the flow speed, made dimensionless using the capillary speed γ/η. Here γ is the coefficient of surface tension between the liquid and an inert exterior gas and η is the shear viscosity of the liquid. This exponential dependence was later verified experimentally by Lorenceau, Restagno & Quéré (2003), using an apparatus similar to that used by Joseph *et al.* (1991) and Jeong & Moffatt (1992).

Cusps play an important role in free-surface flow, because they provide a key mechanism for the entrainment of air into a liquid bath (Kiger & Duncan 2012). Owing to the exponential shrinkage of the tip size with capillary number, the gap inside the cusp becomes extremely narrow. This means that an external fluid (such as air), which is drawn into the cusp, leads to an elevated lubrication pressure inside the narrow gap, which eventually leads to a bifurcation (Eggers 2001; Lorenceau, Quéré & Eggers 2004), even if the viscosity of the outer liquid is much smaller than that of the bath. As a result of the bifurcation, a sheet of air is drawn into the liquid (Lorenceau *et al.* 2004), opening a channel for air entrainment. In the present paper, however, we will disregard the effect of any external fluid, and focus on the formation of the cusp and its relation to the driving flow.

Following Jeong & Moffatt (1992), many more exact two-dimensional solutions similar to theirs were constructed using the method introduced by Richardson (1968), placing various singularities underneath a flat surface (Jeong & Moffatt 1992; Jeong 1999, 2010, 2007), or near a two-dimensional 'bubble' (Antanovskii 1996; Cummings & Howison 1999; Cummings 2000; Crowdy 2002). However, while instructive, no number of exact solutions for a specific geometry and driving explains the mathematical structure of the cusp, and the local balance underlying it. In particular, Jeong & Moffatt (1992) found their interface profile to exhibit the form of a similarity solution near the tip. Its form corresponds exactly to the generic singularity of a planar curve near a point of self-intersection (Eggers & Fontelos 2012, 2015), as found in singularity (bifurcation) theory (Eggers & Suramlishvili 2017).

This suggests that singularities of higher order can also be realised in Stokes flow, and that there are deep connections with other free-surface flows (Eggers & Fontelos 2012), such as Hele-Shaw flow (Howison 1986) or potential flow (Mallet-Paret 1980). This connection has been explored further in a series of papers (Howison & Richardson 1995; Cummings & Howison 1999; Cummings, Howison & King 1999), but always relying on a particular set of exact solutions, furnished by complex mappings. Instead, we aim to understand the structure of the solution in its full generality, relying on local arguments only.

The problem of finding local cusp solutions has recently been addressed by one of us (Eggers 2023), using a boundary integral method. However, the necessary calculations are quite involved, and the integral formulation obscures the simple force balance expressed by the equations of fluid motion. Instead, here we pursue an alternative approach proposed in Morgan (1994), Howison, Morgan & Ockendon (1997) and Gillow (1998), which relies on the slenderness of the cusp, and which has been applied to a wide range of potential flow, Hele-Shaw flow and Stokes flow problems with and without surface tension. The stationary cusp in Stokes flow with surface tension, inspired by the exact solution of Jeong & Moffatt (1992), has, however, not yet been considered in this way.

In the following, we assume that all lengths have been made dimensionless using some external length scale L, which is a feature of the particular geometry of the apparatus at hand. In the example of the solution of Jeong & Moffatt (1992), in which the flow is driven by a vortex dipole underneath a free surface, this could be the depth of the dipole in its rest

https://doi.org/10.1017/jfm.2026.11239 Published online by Cambridge University Press

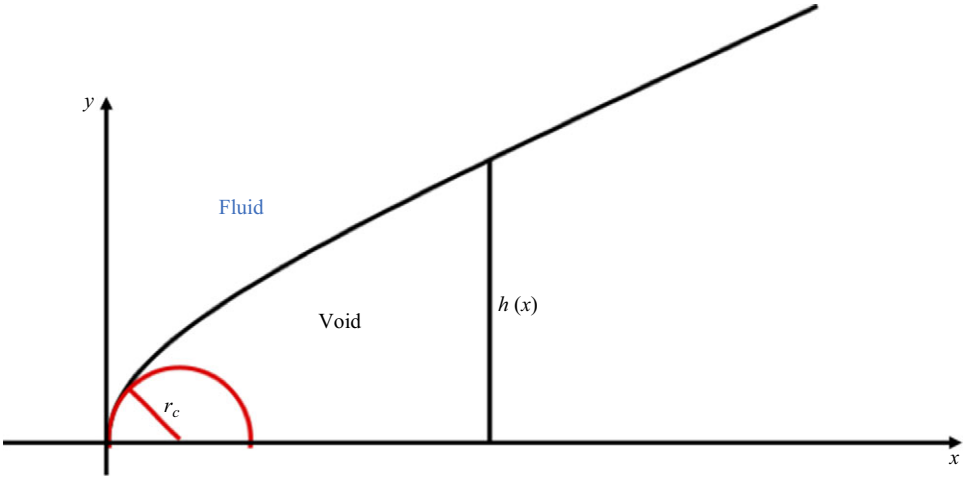

Figure 1. A sketch of the cusp geometry, symmetric about the x axis: the shape is described by $h(x)$, there is a viscous fluid outside and the inside of the cusp contains a gas which does not exert any stress. The tip of the cups is rounded, with r_c the radius of curvature.

state of vanishing dipole strength. Velocities are measured in units of the capillary speed γ/η, so that $\eta L/\gamma$ is a time scale. We are solving the two-dimensional, steady, viscous flow equations with a free surface, written as $y = h(x)$, and assuming symmetry about the x axis (see figure 1). The viscous flow equation in the bulk is

$$\nabla p = \triangle \boldsymbol{v}, \tag{1.1}$$

where $\boldsymbol{v} = (u, v)$ is a two-dimensional velocity field and p the pressure. On the free surface ($\boldsymbol{\sigma}$ is the stress tensor) the stress boundary condition reads

$$\boldsymbol{n} \cdot \boldsymbol{\sigma} = \frac{h''}{\left(1 + h'^2\right)^{3/2}} \boldsymbol{n}, \tag{1.2}$$

where a prime denotes the derivative with respect to the argument and $\boldsymbol{n}$ is the normal to the free surface. The condition for a steady flow is

$$h' = \frac{v}{u}. \tag{1.3}$$

Equations (1.1)–(1.3) have been made dimensionless using the length L, time scale $\eta L/\gamma$ and pressure scale γ/L. We aim to solve (1.1)–(1.3) in the limit that the radius of curvature of the tip r_c (see figure 1) tends to zero.

2. Asymptotic solution

Our solution proceeds by matching two asymptotic regions shown schematically in figure 2. The tip region plays the role of an inner solution, the cusp region is the outer solution. We begin by describing both regions individually, and then show in more detail how they are matched.

2.1. *The tip region*

The tip region has the form of a parabola $h = \sqrt{2r_c}x^{1/2}$, where r_c is the radius of curvature. This shape, together with an appropriate velocity field, is an exact steady solution of the Stokes equation with surface tension (Hopper 1993). This can be shown by solving the

https://doi.org/10.1017/jfm.2026.11239 Published online by Cambridge University Press

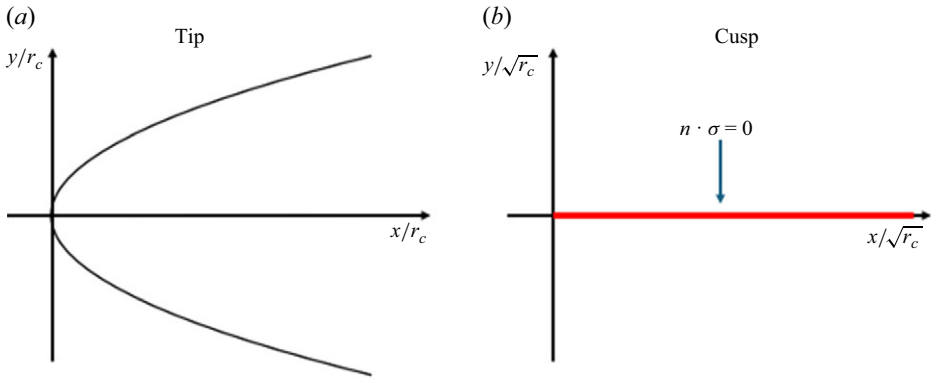

Figure 2. (*a*) The inner (tip) region, which has typical scale r_c; the interface reduces to a parabola in the limit $r_c \to 0$. (*b*) In the outer (cusp) region, the interface reduces to the positive x axis when viewed on scale $\sqrt{r_c}$, with $r_c \to 0$.

equations using the mapping

$$z = 2r_c w(\zeta) \equiv 2r_c \left(\zeta^2 + \mathrm{i}\zeta\right), \tag{2.1}$$

where ζ real corresponds to the free surface. Thus the upper half of the ζ plane is mapped into the fluid domain, which is the outside of the cusp. In the Goursat representation (Jeong & Moffatt 1992), the streamfunction of the flow is written in terms of two holomorphic functions f and g:

$$\psi = \mathrm{Im}\left\{f(z) + \bar{z}g(z)\right\}; \tag{2.2}$$

the components of the velocity field are calculated from $u = \psi_y$ and $v = -\psi_x$, where the subscript denotes the derivative. However, in the complex formulation the velocity field is recovered more conveniently from

$$u - \mathrm{i}v = f'(z) + \bar{z}g'(z) - \overline{g(z)}. \tag{2.3}$$

As shown in Hopper (1993), the steady flow around the parabola (2.1) is given by

$$f = \frac{\mathrm{i}r_c}{2} w'(\zeta)\bar{w}(\zeta)G(\zeta), \quad g = -\frac{\mathrm{i}}{2} w'(\zeta)G(\zeta), \tag{2.4}$$

where

$$G = \frac{1}{2\pi\mathrm{i}\sqrt{1+4\zeta^2}} \ln\left(\frac{2\zeta - \sqrt{1+4\zeta^2}}{2\zeta + \sqrt{1+4\zeta^2}}\right) \tag{2.5}$$

and $\bar{w}(\zeta) = \overline{w(\bar{\zeta})}$ is the conjugate function.

The free surface can be parametrised by putting $\zeta = \phi/2$, with ϕ real, the tangent vector to the parabola is $\boldsymbol{t} = (\phi, 1)/\sqrt{1+\phi^2}$ and thus the tangential velocity u_0 is found from $u_0 = (u\phi + v)/\sqrt{1+\phi^2}$. Using the solution (2.4), this gives

$$u_0(\phi) = -\frac{1}{\pi} \ln\left(\sqrt{1+\phi^2} + \phi\right), \quad \phi = \sqrt{2x/r_c}, \tag{2.6}$$

in agreement with Eggers (2023); the velocity near the interface can be inferred from

$$(u, v) = \frac{(1, h')}{\sqrt{1+h'^2}} u_0. \tag{2.7}$$

https://doi.org/10.1017/jfm.2026.11239 Published online by Cambridge University Press

In the far field, along the interface

$$u_0 = -\frac{1}{2\pi}\ln\frac{8x}{r_c}, \tag{2.8}$$

which is the far field of a stokeslet, i.e. the velocity field generated by a point force of strength 2. This corresponds to each side of the interface pulling with force γ (per unit length in the third direction). Since $h' = \sqrt{r_c/(2x)}$, which vanishes for $x \to \infty$, we have

$$u = -\frac{1}{2\pi}\ln\frac{8x}{r_c}, \quad v = -\frac{\sqrt{r_c}}{2^{3/2}\pi\sqrt{x}}\ln\frac{8x}{r_c}, \tag{2.9}$$

again for large x.

2.2. *The cusp region*

In the cusp region, we can make use of slenderness and model the air gap as a cut in the complex plane along the positive x axis, as illustrated in figure 2(*b*); this is confirmed more formally below. We are seeking solutions to the Stokes equation symmetric about the x axis and with stress-free conditions along the positive x axis, valid locally around the tip of the cusp, which is at the origin. This is justified by the crucial observation that the stokeslet solution does not contribute to the stress at leading order, as we see below.

Since the asymptotic problem of a cut of vanishing thickness is lacking a characteristic length scale, we seek power-law solutions for the streamfunction of the form (Eggers & Fontelos 2015)

$$\psi = r^\lambda\left[A\sin(\lambda\varphi) + C\sin((\lambda-2)\varphi)\right], \tag{2.10}$$

where r is the distance from the tip and φ the angle measured from the negative x axis. This ensures that the line $\varphi = 0$ in the wake of the cusp is a streamline, while the surface of the cusp is at $\varphi = \pi$. Expansions of this form are standard in two-dimensional solid mechanics (see e.g. Muskhelishvili 1953; Gakhov 1966). As shown in detail in Eggers & Fontelos (2015), eliminating the pressure and demanding that the two components of the stress vanish at the free surface $\varphi = \pi$ lead to the conditions $\sin\lambda\pi = 0$ or $\cos\lambda\pi = 0$ for the scaling exponent λ.

The first class of solutions leads to integer λ, with vanishing transversal velocity $v = 0$ along the cusp surface $x > 0$. Non-singular velocity fields correspond to $\lambda = 1, 2, \ldots$, yielding $u = x^n$, $n = 0, 1, \ldots$ for the tangential velocity along the cusp surface. Thus with $-U$ being the leading-order velocity sweeping past the cusp, a general superposition of these solutions yields the tangential velocity

$$u = -U + b_1 x + b_2 x^2 + \cdots, \tag{2.11}$$

with b_i being parameters. On the other hand, the second condition (and avoiding solutions too singular to match to the parabolic solution (2.4)), leads to $\lambda = 1/2, 3/2, \ldots$. Then on the positive x axis, the velocity corresponding to these values is normal to the cusp, so that up to normalisation $u = 0$, $v = \pm x^{(2n-1)/2}$, $n = 0, 1, 2, \ldots$, above and below the gap, respectively. This means a general superposition of normal velocities is of the form

$$u = 0, \quad v = a_0 x^{-1/2} + a_1 x^{1/2} + \cdots, \tag{2.12}$$

once more with a_i as free parameters.

In addition to (2.10), another solution to the Stokes equation in the presence of a gap is a stokeslet of strength unity, pulling in the positive x direction (Pozrikidis 1992):

$$\psi = -\frac{y}{4\pi}\ln(r/a); \tag{2.13}$$

https://doi.org/10.1017/jfm.2026.11239 Published online by Cambridge University Press

a is a positive constant. Solution (2.13) is distinct from (2.11) and (2.12), in that it breaks scale invariance.

Once more both components of the normal stress generated by (2.13) vanish on the surface $y=0$. Now the velocity on the positive x axis corresponding to (2.13) is $u=-\ln(x/a)/(4\pi)$ and $v=0$, which matches (2.9) for a stokeslet of strength 2, and putting $a=r_c/8$. This means that the total tangential component of the velocity is of the form

$$u=-\frac{1}{2\pi}\ln\left(\frac{8x}{r_c}\right)+b_1x+b_2x^2+\cdots. \tag{2.14}$$

The leading-order contribution to (2.12) for which v remains finite at $x=0$ is $a_1x^{1/2}$; this is the one considered in Joseph *et al.* (1991) and Eggers & Fontelos (2015). Together with a constant down-streaming $u=-U$ (which is the leading contribution to (2.11)), this produces a cusp which opens with a $3/2$ exponent. The crucial observation is that in order to match to the parabolic solution, we also have to add $a_0x^{-1/2}$ to obtain

$$u=-U+b_1x,\quad v=a_0x^{-1/2}+a_1x^{1/2}, \tag{2.15}$$

with higher-order terms discarded.

Then since the interface is a streamline in steady state, we obtain for the slope

$$h'=\frac{v}{u}=-\frac{a_0}{U}x^{-1/2}-\left(\frac{a_1}{U}-\frac{a_0b_1}{U^2}\right)x^{1/2}+O\left(x^{3/2}\right). \tag{2.16}$$

Thus identifying

$$r_c=2\left(\frac{a_0}{U}\right)^2,\quad c=-\frac{2a_1}{3U}+\frac{a_0b_1}{U^2}, \tag{2.17}$$

and integrating (2.16), this yields

$$h=\sqrt{2r_c}x^{1/2}+cx^{3/2}, \tag{2.18}$$

which is precisely the self-similar cusp profile found originally by Jeong & Moffatt (1992). Again, higher-order terms have been discarded in order to obtain the leading-order shape valid near the cusp tip. This is the central result of this paper, in which the structure of the cusp is obtained by local analysis of the flow equations alone.

For small x, (2.18) agrees with the parabolic solution (2.1). On the other hand, to leading order as $r_c\to0$, comparing (2.14) and (2.11) provides the down-streaming velocity $U>0$:

$$U=-\frac{1}{2\pi}\ln\frac{r_c}{8}, \tag{2.19}$$

which reveals an exponential dependence of the tip curvature on the externally imposed flow, as found originally by Jeong & Moffatt (1992).

2.3. *Matching*

We now make sure that the solution proposed above is consistent in the limit $r_c\to0$, and that the different parts match. From (2.18) we see that the two terms on the right are balanced for $x=O(r_c^{1/2})$, so that both terms are of $O(r_c^{3/4})$. For x of the order of r_c, we are in the tip region; conversely for x on the scale of $\sqrt{r_c}$, we are in the cusp region, as shown in figure 2. It follows that (2.18) can be written in self-similar form as

$$y=r_c^{3/4}H\left(x/r_c^{1/2}\right),\quad H(\xi)=(2\xi)^{1/2}+c\xi^{3/2}, \tag{2.20}$$

where c remains a free parameter, which depends on the particular problem at hand. The similarity solution (2.20) is precisely of the form found by Jeong & Moffatt (1992) for a

https://doi.org/10.1017/jfm.2026.11239 Published online by Cambridge University Press

vortex dipole underneath an infinitely extended free surface, and thus for a specific value of the constant c only. Our calculation now demonstrates that (2.20) is the generic structure of the cusp, and establishes c as the only free parameter, once the radius of curvature r_c is taken as a reference length scale.

The structure of the matching problem is illustrated in figure 2. In figure 2(a), we show the inner, tip problem, which lives on scale r_c. It represents an exact solution to the Stokes equation with a free surface, which happens to be a parabola. Putting $\bar{x} = x/r_c$ and $\bar{y} = y/r_c$, this free surface can be written as

$$\bar{y} = \sqrt{2\bar{x}}. \tag{2.21}$$

In figure 2(b), we illustrate the outer, cusp solution on scale $\sqrt{r_c}$. It follows from (2.20) that in the limit $r_c \to 0$ the surface degenerates to a line, occupying the positive x axis, shown as the thick red line. Moreover, we show that to leading order the boundary condition on the cut is stress-free, as assumed in deriving solutions (2.11)–(2.13). First, using the scaling (2.20), we estimate the curvature in (1.2) as $\kappa = O(r_c^{3/4}/\sqrt{r_c}^2) = O(r_c^{-1/4})$. Second, to estimate the stress, we note that the stokeslet solution (2.13), for which $v = 0$, does not contribute to the stress. At next order, combining (2.15) and (2.17), we have $v \approx a_0 x^{-1/2} = O(\sqrt{r_c/x}\ln r_c)$. Estimating the derivative at scale $\sqrt{r_c}$, we find

$$\sigma = O\left(\sqrt{r_c/x^3}\ln r_c\right) = O\left(r_c^{-1/4}\ln r_c\right), \tag{2.22}$$

which dominates the curvature by a logarithmic factor, and justifies looking for stress-free cusp solutions. This is a key observation, which explains why in spite of the complexity of the velocity field, which contains logarithmic contributions (e.g. (2.3)), finding cusp solutions reduces to finding solutions to the Stokes equation in the 'cut plane' domain of figure 2.

Finally, we confirm the matching between the inner and outer velocity fields by comparing the outer limit of the inner solution with the inner limit of the outer solution. In the limit $r_c \to 0$,we find from (2.9) (the inner solution):

$$u = \frac{1}{2\pi}\ln\frac{r_c}{8} = -U, \quad v = \frac{\sqrt{r_c}}{2^{3/2}\pi\sqrt{x}}\ln\frac{r_c}{8} = \sqrt{\frac{r_c}{2x}}U, \tag{2.23}$$

using (2.19). If one considers the inner limit of (2.12), one obtains $v = a_1 x^{-1/2} = \sqrt{r_c/2}Ux^{-1/2}$, which is the second equation of (2.23), which demonstrates the required matching.

2.4. *The outer flow*

The flow defined by (2.14) has the property that it is not bounded at infinity, so one might worry that it cannot be matched to a finite outer flow. We now show that this is not a limitation of the present approach. Rather, solutions of the form (2.11) can be superimposed to produce bounded velocities. To see that, it is advantages to use the complex representation (2.2), in which solutions $u = x^n$ are described by

$$f(z) = \frac{z^{n+1}}{2}, \quad g(z) = \frac{z^n}{2}. \tag{2.24}$$

Indeed, the streamfunction is

$$\psi = \frac{1}{2}\mathrm{Im}\{z^{n+1} - \bar{z}z^n\} = y\,\mathrm{Im}\{iz^n\} = yx^n, \tag{2.25}$$

https://doi.org/10.1017/jfm.2026.11239 Published online by Cambridge University Press

so we recover $u = \partial_y \psi = x^n$. Similarly, the streamfunction of a stokeslet (2.13) can be written $\psi = y\,\mathrm{Re}\{\ln z\}$.

Superimposing the solutions (2.25), we can write in general

$$\psi = y\,\mathrm{Re}\{\chi(z)\}, \quad \text{with } \chi(z) = d_0 \ln z + \sum_{n=0}^{\infty} d_{n+1} z^n. \tag{2.26}$$

By choosing

$$\chi(z) = -\frac{1}{2\pi}\ln\frac{8z}{r_c} + \frac{1}{4\pi}\sum_{n=1}^{\infty}(-1)^{n+1}\frac{\mathrm{e}^{-4\pi n U}(8z)^{2n}}{r_c^{2n}} = \frac{1}{4\pi}\ln\left(\mathrm{e}^{-4\pi U} + \frac{r_c^2}{(8z)^2}\right), \tag{2.27}$$

we have constructed a solution which for $z \to 0$ behaves like (2.14). On the other hand, for $z \to \infty$ we have $\chi \approx -U$, implying that a finite tangential velocity $u \approx -U$ is reached at infinity.

Looking at the behaviour of χ in the complex plane, and using (2.19), one obtains

$$\chi = \frac{1}{4\pi}\ln\left(r_c^2 + \frac{r_c^2}{(8z)^2}\right) = \frac{1}{2\pi}\ln\frac{r_c}{8z} + \frac{1}{4\pi}\ln(z-\mathrm{i}) + \frac{1}{4\pi}\ln(z+\mathrm{i}), \tag{2.28}$$

which has logarithmic singularities at $z = \pm\mathrm{i}$, or $y = \pm 1$. According to (2.26), this means that near the singularities

$$\psi = \pm\frac{1}{4\pi}\ln(z \mp \mathrm{i}), \tag{2.29}$$

which are counter-rotating vortices of circulation $\Gamma = \mp 1/2$ situated at $z = \pm\mathrm{i}$. This is very similar to the solution considered in Jeong (2010), where the flow leading to a cusp is driven by a pair of vortices. This, in turn, can be seen as an idealisation of the experimental set-ups in Joseph *et al.* (1991) and Jeong & Moffatt (1992), where the flow is driven by two counter-propagating rollers.

The particular solution considered in (2.27) is just one of the many different ways of driving a free surface to cusp formation. However, a common feature of any such solution is the presence of singularities, of which the two vortices of (2.28) are a particular example. More generally, χ has to satisfy the requirement that $\chi \sim \ln z$ as $z \to 0$, to represent the stokeslet generated at the tip. This implies that $z\chi'(z) \sim 1$ as $z \to 0$: the combination $z\chi'(z)$ is free of singularities at the origin. In addition, the assumed boundedness of the velocity field at infinity implies that $z\chi'(z)$ can only grow sublinearly at infinity.

But supposing that $z\chi'(z)$ is analytic in the entire complex plane implies a contradiction: by Liouville's theorem, such an analytic function has to grow at least linearly at infinity, which would be inconsistent with the velocity remaining bounded. Thus, the existence of singularities inside the flow, such as in (2.28), is a feature of the matching conditions we imposed. There is of course an infinite variety of ways such singularities can be imposed, corresponding to various ways in which the flow is driven.

3. Discussion

3.1. *Higher-order singularities*

The remarkable property of the profile (2.18) is that it corresponds exactly to the generic singularity of a smooth, planar curve, which is being deformed smoothly to produce a self-intersection (Eggers & Fontelos 2015; Eggers & Suramlishvili 2017). At the critical point

https://doi.org/10.1017/jfm.2026.11239 Published online by Cambridge University Press

where intersection first occurs, the curve then produces a cusp $h \propto x^{3/2}$, but the tip remains rounded on a small scale in the neighbourhood of that point. The generic behaviour near such critical points is described by the singularity theory (Arnol'd *et al*. 1993), with the planar case described in more detail in Eggers & Suramlishvili (2017).

We emphasise that the cusp solutions discussed here differ fundamentally from Hopper's solution describing the coalescence of cylinders in viscous flow (Hopper 1990; Eggers, Sprittles & Snoeijer 2025). First, the coalescence solution is time dependent, not stationary, as are our solutions. Second, Hopper's solution is non-generic, in that it applies only to a very specific initial condition, in which two cylinders touch in a perfectly aligned fashion. Third, and most importantly, the similarity solution describing the gap between two coalescing cylinders corresponds to an 'elliptic umbilic catastrophe' (Eggers *et al*. 2025), in the language of catastrophe theory (Poston & Stewart 1978), which differs qualitatively from the cusp solutions associated with self-intersection, considered here.

In the present cusp problem, the symmetry of our problem under reflection suggests putting $x = s^2$, with s parameterising the curve. Then, (2.18) turns into the parameterised curve

$$(s^2, \sqrt{2r_c}s + cs^3). \tag{3.1}$$

Up to a rescaling of the axes, this corresponds to the unfolding of the germ (s^2, s^3) (Eggers & Suramlishvili 2017), the latter being the singular curve at the critical point. The singularity theory demonstrates that up to smooth transformations, any deformation of the original germ can be written in the form $(s^2, \mu_1 s + s^3)$, where μ_1 is a parameter. But this is exactly of the form (3.1), again up to trivial rescaling.

It is surprising that the terms appearing in (3.1) only involve integer powers, as required by the singularity theory. This is a direct result of the fact that the stokeslet (2.13), although nominally the leading-order contribution to the velocity field, ends up making a subdominant contribution to the stress, as demonstrated by the estimate (2.22). As a result, logarithms do not appear in (2.15).

Thus, it is natural to generalise (3.1) to unfoldings of higher order, corresponding to higher-order terms in the sequence of powers appearing in (2.12) and (2.11). For example, if from the solution $v = a_n x^{(2n-1)/2}$ one chooses $n = 2$, and from (2.11) one takes the leading order contribution $u = -U$, one obtains $h' = v/u = -(a_2/U)x^{3/2}$. After integration, we obtain $h = -2a_2/(5U)x^{5/2}$, and hence we have generated the so-called A_4 germ (s^2, s^5) (up to rescaling), discussed in detail in Eggers & Suramlishvili (2017). As this germ is of higher order, one obtains a more general class of unfoldings, which are

$$(s^2, \mu_1 s + \mu_3 s^3 + s^5), \tag{3.2}$$

with two parameters μ_1 and μ_3. But this is precisely the solution of Stokes' equation one obtains when including terms with for $n = 0$, 1, and 2 in the superposition (2.12).

In the generic case, in which $\mu_3 \neq 0$ has a finite value, the s^3 term will dominate over s^5 near the tip of the cusp, and we fall back onto the standard profile (2.18). However, one can aim to adjust experimental conditions to reach a state of higher symmetry, at which the cubic term vanishes. Then, if we fine-tune the external flow such that μ_3 becomes small according to $\mu_3 = -2\sqrt{\mu_1}$ as $\mu_1 \to 0$, a bubble is formed, whose shape is described by

$$(x, y) = (s^2, s(s^2 - \sqrt{\mu_1})^2), \tag{3.3}$$

(see figure 3 left). Similar shapes have been pointed out by Cummings & Howison (1999) (see their figure 2), based on a particular class of exact solutions. The cusp now opens like $h = x^{5/2}$, and the size of the bubble shrinks to zero as $\mu_1 \to 0$. Of course, other

https://doi.org/10.1017/jfm.2026.11239 Published online by Cambridge University Press

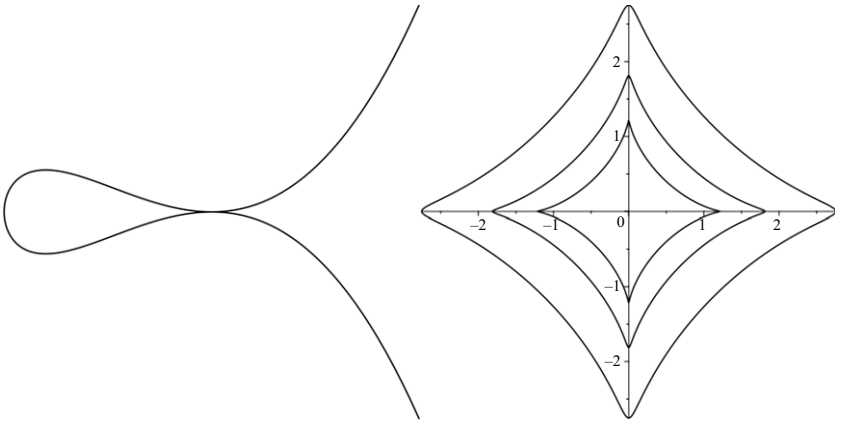

Figure 3. Left: A static solution to the Stokes equation, showing a bubble being enclosed at the tip of a cusp, as described by (3.3). The cusp opens like $h = x^{5/2}$. Right: A shrinking two-dimensional bubble, with a source of unit strength at the centre, as described by (3.4) and (3.6) for $\hat{t} = 2$, 1, and 0.5; the bubble vanishes for $\hat{t} = 0$.

distinguished limits can be realised. A more detailed account of all the different possible structures is given in figure 6 of Eggers & Suramlishvili (2017).

3.2. *Time-dependent solutions*

Our analysis can also be extended to cusps that evolve in time. Examples of such cusps are given by Tanveer & Vasconcelos (1994, 1995), who employed conformal mapping techniques to study cusp formation in contracting bubbles. They were able to derive exact solutions for a two-dimensional bubble driven by a point sink at its centre. The simplest family of such solutions, corresponding to bubbles with $(N+1)$-fold symmetry, is shown on the right of figure 3 for $N = 3$. By taking the real and imaginary parts of Eqs. (84) together with (89) in Tanveer & Vasconcelos (1995), the solutions can be expressed in the parametric form

$$(x^*, y^*) = \sqrt{\frac{\mathcal{A}(t)}{\pi N(N\rho(t)^2 - 1)}}\,(N\rho(t)\cos\theta + \cos(N\theta),\, N\rho(t)\sin\theta - \sin(N\theta)), \quad (3.4)$$

where $-\pi \leqslant \theta < \pi$. Here, (x^*, y^*). is measured from the bubble centre, $\mathcal{A}(t)$ is the area of the bubble at time t, and $\rho(t)$ satisfies a nonlinear ODE, whose asymptotic solution is given below. As the bubble shrinks to zero, the size of the four tips decreases rapidly.

To find a local description near one of the tips, we expand (3.4) about $\theta = 0$, retaining terms up to $O(\theta^3)$, resulting in

$$(x^*, y^*) \approx \sqrt{\frac{\mathcal{A}(t)}{\pi N(N\rho^2 - 1)}}\left(N\rho + 1 - \frac{N\rho + N^2}{2}\,\theta^2,\ (N\rho - N)\theta + \frac{N^3 - N\rho}{6}\,\theta^3\right). \quad (3.5)$$

If lengths are normalised so that the initial bubble area is π and the suction rate is chosen to be unity, $\mathcal{A}(t) = \pi - t$, and the bubble is fully depleted at $t_f = \pi$. Defining $\hat{t} = t_f - t\ (= \mathcal{A}(t))$, Tanveer & Vasconcelos (1995) expanded the exact solution as $\hat{t} \to 0$, showing that

$$\rho(t) \sim 1 + \exp\left(-\frac{2}{(N+1)\hat{t}^{1/2}}\sqrt{\frac{\pi N}{N-1}}\right) \quad (3.6)$$

https://doi.org/10.1017/jfm.2026.11239 Published online by Cambridge University Press

(see Eqs. (89) and (97) of Tanveer & Vasconcelos (1995)). Substitution into the local expansion (3.5) yields

$$(x^*, y^*) \sim \sqrt{\frac{\hat{t}}{\pi N(N-1)}} \left(N + 1 - \frac{N+N^2}{2}\theta^2, N \exp\left(-\frac{2}{(N+1)\hat{t}^{1/2}} \sqrt{\frac{\pi N}{N-1}} \right) \theta + \frac{N^3 - N}{6}\theta^3 \right), \tag{3.7}$$

where, in each monomial in θ, only the dominant term in $\hat{t}$ has been kept.

Upon shifting the axes such that the right-hand cusp tip is at the origin, rescaling the axes, and absorbing the time-independent factor $1/(8(N+1))\sqrt{(N/(\pi(N-1)))}$ into the lengthscale, (3.7) can be recast in the form (2.18), with

$$h = 4\hat{t}^{1/4} \exp\left(-\frac{2}{N+1} \sqrt{\frac{\pi N}{N-1}} \hat{t}^{-1/2} \right) x^{1/2} + \frac{1}{6}\frac{N-1}{N+1}\hat{t}^{-1/4}x^{3/2}. \tag{3.8}$$

The coefficient of the $x^{1/2}$ term, corresponding to $\sqrt{2r_c}$ in (2.18), goes to zero exponentially fast as $\hat{t} \to 0$, thus demonstrating the approach to a singular cusp, as illustrated in figure 3.

The profile (3.8) can be understood in the light of the local description of § 2.2. First, since the area of the bubble decreases linearly in $\hat{t}$, the natural lengthscale for the size of the bubble (the outer region) is $L \propto \hat{t}^{1/2}$. To remove this implicit time dependence, we rescale the local variables as $h \mapsto \hat{t}^{1/2}h$ and $x \mapsto \hat{t}^{1/2}x$, such that (2.18) becomes

$$h = \sqrt{2r_c}\hat{t}^{1/4}x^{1/2} + c\hat{t}^{-1/4}x^{3/2}. \tag{3.9}$$

Furthermore, since the outer flow is driven by a point sink, velocities scale as $1/L \propto \hat{t}^{-1/2}$. To account for this, we rescale the velocity field according to $(u, v) \mapsto \hat{t}^{-1/2}(u, v)$. With this rescaling, (2.19) gives $r_c = 8\exp(-2\pi U\hat{t}^{-1/2})$, where U is independent of time. Substituting r_c into (3.9) yields

$$h = 4\hat{t}^{1/4} \exp(-\pi U\hat{t}^{-1/2})x^{1/2} + c\hat{t}^{-1/4}x^{3/2}, \tag{3.10}$$

which agrees with (3.8). Note that while the determination of U and c requires the solution of the outer problem (or comparison with (3.8)), the asymptotic description captures both the geometry and temporal evolution of the cusp.

This shows that our analysis extends naturally to unsteady problems, provided the coefficients are allowed to vary in time. To properly justify that, note that unsteadiness enters only through the kinematic boundary condition, which for small slopes reads $h_t = v - uh'$. For the time-dependent cusps discussed above, we have $h_t = O(h/\hat{t})$ and $uh' = O(h/(\hat{t}^{1/2}\sqrt{r_c}))$. In the latter expression, we used that the velocity scales as $\hat{t}^{-1/2}$ and that the cusp lengthscale is $\sqrt{r_c}$, as shown in § 2.2. Since r_c is exponentially small in $\hat{t}$, the advective term uh' dominates h_t, hence the leading-order balance reduces to $v = uh'$, and the cusp dynamics is therefore quasi-steady. In view of this, we expect the same framework to describe other types of time-dependent cusps, such as those in figure 5 of Tanveer & Vasconcelos (1995), where a small bubble is enclosed at the tip, which appears to be analogous to the cusp on the left of figure 3.

Finally, another generalisation is to consider departures from exactly two-dimensional flow: this is easily built in by allowing μ_1 to be a function of a third variable z. As long as this variation takes place on a scale much smaller than the tip curvature, the above asymptotics will remain valid and will describe a three-dimensional flow to leading order.

https://doi.org/10.1017/jfm.2026.11239 Published online by Cambridge University Press

Funding. M.F. acknowledges financial support through grant PID2023-150166NB-I00.

Declaration of interests. The authors report no conflict of interest.

References

ANTANOVSKII, L.K. 1996 Formation of a pointed drop in Taylor's four-roller mill. *J. Fluid Mech.* **327**, 325.

ARNOL'D, V.I., VASIL'EV, V.A., GORYUNOV, V.V. & LYASHKO, O.V. 1993 Singularity theory II: classification and applications. In *Dynamical Syatems VIII*, chap. 2. Springer.

CROWDY, D. 2002 Exact solutions for two steady inviscid bubbles in the slow viscous flow generated by a four-roller mill. *J. Engng Maths* **44**, 311.

CUMMINGS, L.J. 2000 Steady solutions for bubbles in dipole-driven Stokes flows. *Phys. Fluids* **12**, 2162.

CUMMINGS, L.J. & HOWISON, S.D. 1999 Two-dimensional Stokes flow with suction and small surface tension. *Eur. J. Appl. Maths* **10**, 681–706.

CUMMINGS, L.J., HOWISON, S.D. & KING, J.R. 1999 Two-dimensional Stokes and Hele-shaw flows with free surfaces. *Eur. J. Appl. Maths* **10**, 681–706.

EGGERS, J. 2001 Air entrainment through free-surface cusps. *Phys. Rev. Lett.* **86**, 4290–4293.

EGGERS, J. 2023 Viscous free surface cusps - local solution. *Phys. Rev. Fluids* **8**, 124001.

EGGERS, J. & FONTELOS, M.A. 2012 Cusps in interfacial problems. *Panoramas et Synthèses* **38**, 69–90.

EGGERS, J. & FONTELOS, M.A. 2015 *Singularities: Formation, Structure, and Propagation*. Cambridge University Press.

EGGERS, J., SPRITTLES, J.E. & SNOEIJER, J.H. 2025 Coalescence dynamics. *Annu. Rev. Fluid Mech.* **57**, 61.

EGGERS, J. & SURAMLISHVILI, N. 2017 Singularity theory of plane curves and its applications. *Eur. J. Mech. B* **65**, 107–131.

GAKHOV, F.D. 1966 *Boundary Value Problems*. Pergamon Press.

GILLOW, K. 1998 Codimension-two free boundary problems. PhD thesis, Oxford University, England.

HOPPER, R.W. 1990 Plane Stokes flow driven by capillarity on a free surface. *J. Fluid Mech.* **213**, 349.

HOPPER, R.W. 1993 Capillarity-driven plane Stokes flow exterior to a parabola. *Q. J. Mech. Appl. Maths* **46**, 193.

HOWISON, S.D. 1986 Cusp development in Hele-Shaw flow with a free surface. *SIAM J. Appl. Maths* **46**, 20.

HOWISON, S.D., MORGAN, J.D. & OCKENDON, J.R. 1997 A class of codimension-two free boundary problems. *SIAM Rev.* **39**, 221–253.

HOWISON, S.D. & RICHARDSON, S. 1995 Cusp development in free boundaries, and two-dimensional slow viscous flows. *Eur. J. Appl. Maths* **6**, 441–454.

JEONG, J.-T. 1999 Formation of cusp on the free surface at low Reynolds number flow. *Phys. Fluids* **11**, 521.

JEONG, J.-T. 2007 Free surface deformation due to a source or sink in Stokes flow. *Eur. J. Mech. B/Fluids* **26**, 720.

JEONG, J.-T. 2010 Two-dimensional Stokes flow due to a pair of vortices below the free surface. *Phys. Fluids* **22**, 082102.

JEONG, J.-T. & MOFFATT, H.K. 1992 Free-surface cusps associated with a flow at low Reynolds numbers. *J. Fluid Mech.* **241**, 1–22.

JOSEPH, D.D., NELSON, J., RENARDY, M. & RENARDY, Y. 1991 Two-dimensional cusped interfaces. *J. Fluid Mech.* **223**, 383–409.

KIGER, K.T. & DUNCAN, J.H. 2012 Air-entrainment mechanisms in plunging jets and breaking waves. *Annu. Rev. Fluid Mech.* **44**, 563–596.

LORENCEAU, E., QUÉRÉ, D. & EGGERS, J. 2004 Air entrainment by a viscous jet plunging into a bath. *Phys. Rev. Lett.* **93**, 254501.

LORENCEAU, É., RESTAGNO, F. & QUÉRÉ, D. 2003 Fracture of a viscous liquid. *Phys. Rev. Lett.* **90**, 184501.

MALLET-PARET, J. 1980 Generic bifurcation in the obstacle problem. *Q. Appl. Maths* **37**, 355–387.

MORGAN, J.D. 1994 Codimension-two free boundary problems. PhD thesis, Oxford University, England.

MUSKHELISHVILI, N.I. 1953 *Some Basic Problems of the Mathematical Theory of Elasticity*. P. Noordhoff.

POSTON, T. & STEWART, I. 1978 *Catastrophe Theory and its Applications*. Dover Publications.

POZRIKIDIS, C. 1992 *Boundary Integral and Singularity Methods for Linearized Flow*. Cambridge University Press.

RICHARDSON, S. 1968 Two-dimensional bubbles in slow viscous flows. *J. Fluid Mech.* **33**, 476.

TANVEER, S. & VASCONCELOS, G.L. 1994 Bubble breakup in two-dimensional Stokes flow. *Phys. Rev. Lett.* **73**, 2845.

TANVEER, S. & VASCONCELOS, G.L. 1995 Time-evolving bubbles in two-dimensional Stokes flow. *J. Fluid Mech.* **301**, 325.

https://doi.org/10.1017/jfm.2026.11239 Published online by Cambridge University Press